Pancake ice formation in the Weddell Sea

Martin J. Doble[1]
Scottish Association for Marine Science, Dunstaffnage Marine Laboratory, Oban, Argyll, UK

Max D. Coon
North West Research Associates, Inc., Bellevue, Washington, USA

Peter Wadhams[1,2]
Scottish Association for Marine Science, Dunstaffnage Marine Laboratory, Oban, Argyll, UK

Received 5 March 2002; revised 29 December 2002; accepted 3 March 2003; published 1 July 2003.

[1] The ice formation resulting from two low temperature events at the Weddell Sea ice edge during April 2000 is presented. Pancake and frazil ice were sampled at seven stations at varying distances from the ice edge. The ice cover was further characterized from above, using helicopter aerial photography, and from below, using a remotely operated vehicle. Previously undescribed two-layer pancake types were observed and classified. A novel pancake growth mechanism is introduced to account for these, involving the washing of frazil ice over the pancake top surface and its subsequent freezing. The process was directly observed in ice tank experiments. Layer thicknesses seen in the field were compared to the ice growth that would occur both under calm conditions and from free-surface frazil ice growth. Classical, bottom accretion, pancake growth was found to proceed at a rate similar to that of thin congelation ice. Top-layer growth was more rapid, at approximately double the congelation rate. Overall ice volume production was similar to congelation ice for the thin pancakes considered (~20 cm), though subsequent thickening was expected to be faster as the rapid top-layer process continued and the equivalent congelation growth slowed. It is suggested that parameterization of this new process is important for models that aim to simulate the rapid advance and thickening of wave-influenced ice covers. *INDEX TERMS:* 4207 Oceanography: General: Arctic and Antarctic oceanography; 4540 Oceanography: Physical: Ice mechanics and air/sea/ice exchange processes; 9310 Information Related to Geographic Region: Antarctica; *KEYWORDS:* pancake ice, frazil ice, ice formation

Citation: Doble, M. J., M. D. Coon, and P. Wadhams, Pancake ice formation in the Weddell Sea, *J. Geophys. Res.*, *108*(C7), 3209, doi:10.1029/2002JC001373, 2003.

1. Introduction

[2] The formation of Antarctic sea ice in winter is one of the largest seasonal events on the planet, yet the processes by which it forms, especially in the ice edge region, are poorly constrained. Cooling of the ocean surface seaward of the summer ice edge begins to freeze the surface waters but the high turbulence levels of the Southern Ocean do not allow this ice to congeal into a coherent sheet. Ice instead forms as a suspension of unconsolidated crystals, known as frazil or grease ice. These are mixed down into the water by the ocean wind and wave fields, allowing the continued exposure of sea surface to the colder air and the maintenance of a high ocean-atmosphere heat flux. The suspension gradually consolidates into small cakes, known as "pancake ice," by the agglomeration of the frazil crystals. This is assumed to occur both from below and laterally as the buoyant crystals rise to the surface, with the consolidation being driven by the temperature gradient to the cold atmosphere. The frazil crystals are sintered together at their point of contact, minimizing their surface free energy [*Martin*, 1981]. This overcomes their noted reluctance to stick together, caused by an enveloping layer of brine [*Hanley and Tsang*, 1984], contrasting with the behavior of freshwater frazil crystals which rapidly form relatively strong aggregations or "flocs" [*Martin*, 1981].

[3] The pancakes are initially only a few centimeters in diameter and are known as "shuga" in their earliest agglomerations [*Armstrong et al.*, 1973] or "dollar pancakes" [*Wadhams and Wilkinson*, 1999] as the disc form becomes more pronounced. As the penetrating wavefield is damped with distance from the ice edge the pancakes increase in size up to 5 m diameter and more than 50 cm thickness. Only at a considerable distance from the ice edge, up to 270 km [*Wadhams et al.*, 1987], is the ocean swell damped enough to allow the pancakes to freeze together to form a continuous ice sheet, termed "consolidated pancake

[1] Formerly at Scott Polar Research Institute, University of Cambridge, Cambridge, UK.
[2] Also at Department of Applied Mathematics and Theoretical Physics, University of Cambridge, Cambridge, UK.

0148-0227/03/2002JC001373

ice.'' This then thickens, by the usual processes of congelation ice growth on its underside and snowfall on its upper surface, to form the familiar pack ice.

[4] The pancake cycle thus exerts a dominant influence on Antarctic ice types [*Weeks*, 1998], and textural investigations of ice in the central Weddell Sea have revealed that pancake ice growth is the dominant mechanism for pack ice formation in this area [*Clarke and Ackley*, 1984; *Gow et al.*, 1987; *Lange et al.*, 1989; *Lange and Eicken*, 1991]. The importance of pancake ice formation lies in the fact that an ice cover of reasonable thickness can establish itself despite a high oceanic heat flux [*Squire*, 1998]. The ice growth is thought to occur at near the open water rate [*Wadhams et al.*, 1987], though quantitative estimates of growth rates during pancake formation are lacking. Once the cover cements together to become continuous, growth drops rapidly to the low levels consistent with an ~50 cm thick ice cover. This subsequent rate is in fact almost zero in the Weddell Sea since the oceanic heat flux then almost balances the loss by conduction through the ice [*Gordon and Huber*, 1990]. *Wadhams et al.* [1987] estimated that only 4 cm of further ice growth took place after the pancake ice cover consolidated.

[5] This paper sets out measurements performed in the pancake zone of the central Weddell Sea, aimed at elucidating these initial ice formation processes and providing a first quantitative estimate of pancake ice growth rates. Previously undescribed pancake morphologies are discussed and a new growth mechanism is introduced to account for these, supported by direct observations from ice tank experiments. Growth periods contributing to pancake building are identified and the rate of pancake formation compared to that which would have occurred by congelation ice growth and frazil ice production at a free surface, calculated using a kinematic-thermodynamic model.

2. Characterization of the Experimental Area

2.1. Location

[6] The experiment took place during the ANT-XVII/3 cruise leg of the Alfred Wegener Institute (AWI) research vessel *Polarstern*, during 5 days in mid-April 2000 [*Doble et al.*, 2001]. The experimental area straddled the 100-km-wide marginal ice zone (MIZ) in the center of the Weddell Gyre, from the ice edge to just seaward of the transition region between pancake and pack ice. Six sampling locations formed a trapezoidal area of dimensions 80 km perpendicular to the ice edge and 110 km parallel to the edge, centered at 68°41′S, 32°32′W. A seventh location was sampled 310 km further west. Drifting buoys, designed to mimic the drift characteristics of pancake ice and carrying a full suite of meteorological sensors, were deployed at each station.

[7] The study period represents a hiatus in the advance of the ice edge. The edge advanced steadily northward in the area of interest, from 71°S on day 77 (March 17) to 69°S by day 91 (March 31). The ice edge between 30°W and 35°W then oscillated between 69°24′S and 68°S, showing no net advance in the next 30 days. West of 35°W and east of 25°W, however, the advance continued, leading to the experimental area becoming semi-enclosed inside a bay-like feature. Rapid growth of the ice edge was then observed, advancing from 68°S to 64°S in 5 days as this bay froze over. Though the embayment is an unusual feature, the ice limit is normal for the season [*Gloersen et al.*, 1992]. The overall behavior is illustrated in Figure 1, which contours the 60% ice concentration limit from mid-March to May and marks the location of experimental stations.

[8] CTD profiles taken in the area showed a mixed layer salinity of 34.35 psu within 0.01°C of its freezing point. Mixed layer depth was approximately 60 m, indicating that the maximum winter depth had not yet been achieved, as expected.

[9] Meteorological conditions during April 2000, derived from the European Centre for Medium-range Weather Forecasts (ECMWF) analyses [*ECMWF*, 1997], show two periods of low air temperature and high wind. These occurred on days 98–101.5 (April 7–10) and 106–108 (April 15–April 17), hereinafter referred to as ''event 1'' and ''event 2,'' respectively. They were separated by a period of calm and relatively high air temperatures (−3°C); conditions which also characterized the sampling period directly following event 2 (days 107.5–110.5 (April 16–April 19)). Weather conditions were therefore extremely fortunate, not only in relation to working conditions on deck, as they represented two distinct ice formation events separated and followed by essentially ''steady state'' periods during which ice neither melted or grew significantly. This allowed the date of frazil and pancake ice formation in the region to be determined with some degree of confidence.

2.2. Ice Cover

[10] Vast fields of frazil ice were observed along the ice edge on day 106 (April 15) for more than 2° of longitude. The frazil fields consolidated overnight and were observed as young, wet pancakes during a helicopter flight the following day. The resulting outer ice cover was extremely diffuse, with a very slow reduction in frazil or young pancake concentration to the north. The term ''ice edge'' is therefore rather subjective, and in this study was taken as the point at which the ice cover became so diffuse that damping of incident swell waves was considered negligible. The outer stations (1 and 4) were performed within 15 km of this line. Mature pancakes upward of 1 m diameter formed the remainder of the study area, from a penetration of approximately 54 km to 95 km from the ''edge.'' The first inner station (2) was performed to the south of the new frazil formation zone (~94 km penetration), and no frazil was seen in this area. Consolidated pack ice was found at 10–15 km further penetration from the line joining the two inner stations.

[11] Areal coverage of each ice type was determined from aerial photography transects flown at each study site to provide continuous overlapping image swaths. The 70-mm negatives were scanned and analyzed using the freeware ''Scion Image'' program. Ice type coverage at each station is shown in Table 1.

[12] The final station (6), to the west of the main area, took place within 4 km of the ice edge, though this was of an entirely different character since the cover had been compacted southward into a sharply defined edge by an approaching deep low pressure. This pressure system had

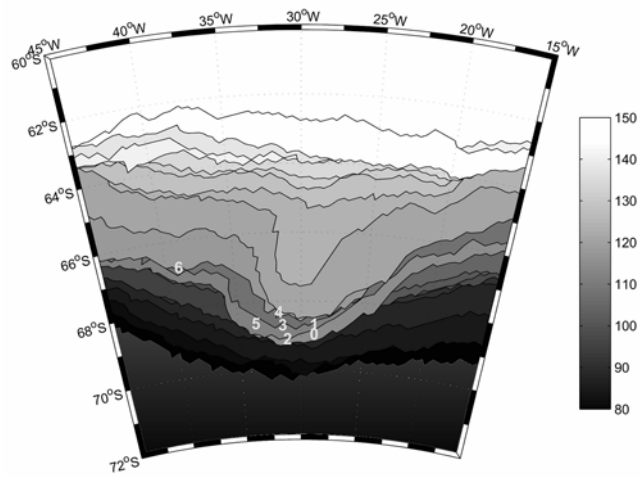

Figure 1. Advance of the ice edge in the experimental area, as shown by the position of the 60% ice concentration limit derived from passive microwave satellite images. The grayscale shows the Julian Day corresponding to each contour, ranging from day 80 (March 20) to day 150 (May 29). The locations of the ice stations (0–6) are marked in white. These took place from day 107 to 111 (April 16–20).

not yet begun to influence the main area during the study, though subsequent rapid southerly movements of the drifting buoys confirmed that this occurred shortly after *Polarstern* left the region.

2.3. Ice Measurements

2.3.1. Methods

[13] Pancake ice was lifted on board using a 1-m^2 "ice basket" and *Polarstern*'s aft crane. The basket retained seawater in its lower section to minimize brine drainage and temperature changes in the recovered pancake before sectioning. Once on deck and removed from the basket, the pancakes were immediately cut in two along one diameter. A vertical temperature profile was then taken down the center of one half, using an electronic probe thermometer inserted to several centimeters depth from the exposed wall at 5-cm intervals. Ice samples were then quickly taken and bottled for later salinity analysis, as described by *Wadhams et al.* [1996]. Samples were also taken from the top surface and rim if the pancake had not been submerged during the lifting process. All sampling was done as quickly as possible to minimize brine drainage during the sampling process, though it is accepted that some drainage is inevitable. A remotely operated vehicle (ROV), carrying an upward-looking video and 35-mm still camera, was deployed at three stations (0, 4, and 6) to verify that the pancakes sampled were representative of the general pancake population.

[14] The frazil ice filling the interstices between pancakes was also sampled, using the ship's "mummy chair" and aft crane. Sampling was done using a 30-cm length of polythene tubing, 8 cm in diameter, with slots cut in the side and open base covered by 300-μm plankton netting. The device was weighted to allow it to sink through thick frazil layers. Sampling was done by dropping the device down through the frazil, moving it to one side and pulling it up through the frazil slush. Water drained through the plankton mesh and the resulting frazil crystals were bottled, melted and analyzed for salinity and melted volume.

2.3.2. Results

[15] A total of 36 pancakes were lifted at seven stations, and their properties are detailed in Table 2. The pancakes presented some unusual morphologies which have not previously been described in the literature. They were divided into six classes depending on their major features, and example photographs of each type are shown in Figure 2. Type A describes the "classic" pancake form: largely flat or saucer-shaped, with lesser or greater development of raised rims. Stations 1 and 4 (the outer ice-edge locations) consisted entirely of this type. Type B pancakes had a characteristic two-layer structure, with the bottom layer formed from frazil ice retaining a high porosity similar to the overlying layer. Salinities of lower and upper layer were very similar for this type, though a clear "step" between the two layers existed, the upper layer having a larger diameter than the lower. Type C pancakes had a frazil-grown lower layer of significantly lower porosity than the overlying layer and were found exclusively at station 6. These layers displayed a lower salinity than the upper layer (e.g., 3.2 psu versus 5.6 psu) and were also clearly stepped. Type D pancakes had a bottom layer of columnar ice up to 44 cm thick, which often displayed open, rotted brine channels. Vertical temperature profiles throughout type D pancakes were essentially isothermal, indicating that the columnar ice was not actively growing. A clear demarcation existed, both externally and in section, between the bottom and the overlying frazil-grown layer, with the now-familiar step being particularly marked. Salinities of the lower layers of this type were again much lower than their overlying layers (e.g., 3.7 psu versus 6.3 psu). Examples were found at all stations other than the two ice-edge locations. Top layers of all two-layer types were commonly wedge-shaped, as can be seen in the photographs of Figure 2, with the top surface at a considerable angle to the bottom surface of the pancake. Type E pancakes are formed as an agglomeration of smaller pancakes, and type F pancakes are rafted. The ROV flights showed that the proportion of rafted pancakes was low in the experimental area, other than in the immediate area beside the ship where they had been pushed aside by the hull. It should be emphasized that no difference between types A-D could be discerned from visual examination of their top surfaces from the ship.

[16] Samples taken from the very top surface of the pancakes were always markedly more saline than the body of the pancake itself, usually double the bulk value or

Table 1. Fractional Area Coverage of Ice Types at Each Sampling Station[a]

Station	f_p	f_f	f_{ow}	f_{floe}
0	0.55	0.35	0	0.10
1	0.60	0.35	0.05	0
2	0.60	0	0.20	0.20
3	0.55	0.30	0.05	0.10
4	0.50	0.40	0.10	0
5	0.65	0.30	0	0.05
6	0.45	0.40	0	0.15

[a]Ice types are classified as pancakes, f_p; frazil, f_f; open water, f_{ow}, and thin congelation ice or older consolidated floe pieces, f_{floe}.

Table 2. Summary of Measurements for the 36 Sampled Pancakes[a]

Station	Number	Type	h_{top}, cm	h_{bottom}, cm	S_{top}, psu	S_{bottom}, psu
0	1	B, E	15	10	12.9	12.5
0	2	D	9	44	–	5.1
0	3	D	22	22	7.6^{2}	3.7
0	4	B	20	6	–	–
1	5	A	5	NA	11.6	NA
1	6	A	8	NA	11.8	NA
1	7	A	7	NA	11.6	NA
1	8	A	7	NA	12.8^{10}	NA
1	9	A	5	NA	13.0	NA
2	10	D	29	20	–	4.5
2	11	D	25	25	6.3	2.4
2	12	D	23	35	–	5.2
2	13	D	27	17	10.9	4.8
2	14	D	20	15	6.8^{14}	6.4^{5}
3	15	D	19	33	–	–
3	16	D	27	29	11.7	4.2^{3}
3	17	B, F	?	?	–	–
3	18	A	9	NA	–	NA
3	19	B, F	12	6	–	–
3	20	D, F	19	22	–	–
3	21	D	15	26	–	–
4	22	A	11	NA	–	NA
4	23	A, E	10	NA	–	NA
4	24	A	10	NA	11.1^{7}	NA
4	25	A	11	NA	–	NA
4	26	A	9	NA	–	NA
5	27	B	14	6	–	–
5	28	D	?	?	–	–
5	29	B	20	10	–	–
5	30	B, F	20	9	–	NA
5	31	D	21	14	–	–
6	32	C	25	23	11.7	–
6	33	C	16	16	13.1	3.6^{2}
6	34	C	22	17	6.7	3.2
6	35	C	18	14	–	–
6	36	C	25	10	–	–

[a]Type refers to the classification given in Figure 2 Thickness h (cm) and salinity S (psu) are given for both pancake layers, where present, with NA (not applicable) entered for the lower layer measurements of single-layer pancake types. A dash indicates that no measurement was taken. Superscripts next to salinity measurements refer to the number of samples contributing to this figure (one, if not indicated). Rim and surface salinity measurements are excluded. Question marks in the thickness columns indicate that the complicated pancake structure made attribution of the layers unreliable.

greater (e.g., 15.2 psu versus 6.4 psu). Rim salinities were comparable to the upper bulk layer (e.g., 6.0 psu versus 5.6 psu). The bulk salinities of the pancake ice formed at each station rank with distance from the ice edge: the outer stations (0, 1, and 4) have the highest salinities at 11.0, 12.5 and 11.1 psu respectively, the middle station (3) has an intermediate salinity (8.2 psu) and the inner ice edge stations (2 and 5) have the lowest (6.4 and 5.4 psu).

[17] A total of 70 frazil samples were taken. Frazil salinities were invariably greater than that of pancakes recovered at the same location. The youngest pancakes, at stations 1 and 4, had salinities approximately 5 psu lower than the corresponding frazil. Frazil salinities ranged from 9.5 psu (station 6) to 18.9 psu (station 1). Frazil salinities were consistent within a station while displaying distinct differences between stations. This coherence at a particular station suggests that the sampling method was consistent, though the mechanism behind these salinity differences is currently unclear. It is interesting to note that the mean frazil salinities at a station tend to indicate its distance from the ice edge; with the outer stations most saline and intermediate stations (0, 3) also fitting the pattern. No frazil was present at the first inner station (2), and the second inner station (5) is the only one not to fit the pattern, having a mean frazil salinity higher than that for the intermediate station 3 (14.2 psu versus 11.7 psu).

2.3.3. Discussion

[18] The greater salinity of the current study's upper pancake layers compared to their lower (observed in all cases) contrasts with previous pancake measurements, performed in the Odden region of the Greenland Sea during winter cruises in 1993, 1997, and 2000 [*Wadhams et al.*, 1996; *Wadhams and Wilkinson*, 1999]. Those pancakes displayed increasing salinity with distance from the top surface, consistent with the classic bottom accretion process. The salinity of the pancake falls rapidly after formation since its highly porous structure allows unimpeded gravity-driven brine drainage [*Tison and Verbeke*, 2001]. The underside remains the most saline, however, since the enveloping layer of brine around those frazil crystals has had less time to drain. Meltwater and rainwater flushing also occurs in the Odden region [*Wadhams and Wilkinson*, 1999], due to air temperatures frequently rising above

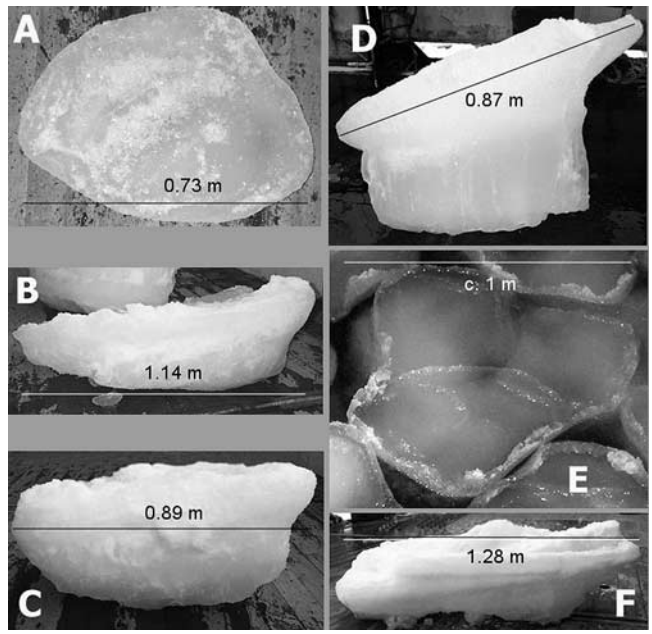

Figure 2. Photographs of pancakes classified according to the scheme adopted in the text, with scale indicated. The pictures show, from top left, Type A: the classic pancake, formed from cyclic accretion of frazil ice (top view, pancake 7); Type B: a pancake having a highly porous lower layer, similar to the overlying layer (side view, pancake 17); Type C: a pancake with a low-porosity bottom layer, representing an older pancake on top of which the younger top layer has been formed (side view, pancake 34); Type D: a pancake with a columnar ice bottom layer (side view, pancake 12); Type E: a pancake formed from an agglomeration of two or more similar pancakes (oblique view of the Station 1 ice cover); and Type F: a pancake with rafted pancakes included (side view, pancake 30).

0°C, and reinforces the characteristic profile. Odden pancakes were apparently all single-layer types (excluding simple rafted examples). The unusual structure of the Weddell Sea pancakes in relation to this well-understood morphology therefore brings into question the bottom accretion process as the sole formation method.

[19] The higher salinity of the upper layer is not unusual for consolidated Weddell Sea pack ice; *Eicken* [1992] found this to be the most common salinity profile, calling such profiles "S type" or "I type." This profile arises since the salinity of congelation ice is closely related to its growth velocity [*Cox and Weeks*, 1988] and the initial, fastest, growth results in the highest salinity ice. Top-layer salinity enhancement can also occur by upward brine expulsion and impeded brine drainage from later top-layer accretions such as snow ice formation, which is common in the Weddell Sea [*Lange et al.*, 1990]. The post-consolidation evolution of the ice tends to blur any salinity contrasts within the original layers, giving similar profiles for largely frazil-grown (granular) ice or dominantly congelation ice cores. These top-layer salinity enhancement processes do not occur in unconsolidated, growing pancakes, however. Individual frazil crystals reject most of their brine in their buoyant ascent to the bottom surface of the slick [*Ushio and Wakatsuchi*, 1993], and the pancake is thus built from relatively constant salinity material. No significant snow deposit was observed on the pancakes and no barrier exists to brine drainage through the pancake, except perhaps in the case of type D pancakes.

[20] The most compelling evidence of the top-down formation mechanism comes from the morphologies. The type D pancakes are particularly striking, since no mechanism exists whereby 44 cm of congelation ice can form beneath a frazil-grown layer whose salinity and porosity suggest it is only a few days old at most. The relative layer porosities observed in type C pancakes are also reversed from the expected bottom accreted types, which typically have a "slushy" bottom surface and hard top surface [*Shen et al.*, 2001]. We therefore postulate that existing pieces of ice act as platforms for the accretion of a younger top layer. That platform can variously be an existing, much older pancake (resulting in a type C composite) or a thin columnar ice piece (giving a type D pancake). Type B pancakes represent a midpoint between type A and type C, since frazil rafting can commence as soon as a type A pancake has grown to sufficient strength to act as a rigid platform without breaking. This explains the lack of contrast between the porosities of bottom and top layers seen in type B pancakes, since the age difference between the layers is small. The mechanism is conceptually similar to the more familiar rafting process, though in this case the overriding ice is unconsolidated frazil rather than a solid ice piece. The top growth mechanism is elegant, since it results in a coherent "family" of pancakes. The bottom accretion mechanism is inconsistent with the salinity and temperature profiles and cannot account for the observed morphologies.

[21] Top-layer growth of pancakes has been directly observed under laboratory conditions in recent ice-tank experiments at the HSVA "Arctelab" facility in Hamburg, Germany, as part of the INTERICE program [*Thomas and Wilkinson*, 2001]. Congelation ice pieces, formed overnight in the still tank, were placed in the wave-influenced area during the next day's pancake ice growth. Frazil ice accretion occurred rapidly on top of these platforms, forming type D pancakes. This top layer was considerably thicker than the conventional (type A) pancake growth which occurred alongside over the same period (thickness 2 cm versus 0.5 cm for the type As). Salinity of the two type D layers showed similar contrast to those in the field, at 15 psu upper versus 11.9 psu lower. Type B/C pancakes were also commonly observed in the tank, and Figure 3 illustrates one such example, clearly showing the more open, porous, top layer. The top surface of pancakes observed in the ice tank was invariably wet (personal observation), indicating a constant supply of water, and hence frazil, to the top surface. The alternative explanation of this wet surface, melting due to elevated salinity, is discounted, since it would have required a surface salinity of over 150 psu in the ~ -10°C air temperatures present in the tank; an order of magnitude greater than measured.

Figure 3. Photograph of a type C pancake grown in the HSVA ice tank. The horizontal line divides the more open, porous, top layer from the more consolidated lower layer.

3. Modeling Layered Pancake Growth

[22] To further support this overtopping hypothesis and establish its rate relative to other forms of ice growth, the formation of the layers was examined with reference to an ice model. We attempt to reproduce the two-layer structures by identifying distinct growth events from the meteorological record and growing ice layers accordingly. We expect the two mechanisms of pancake layer growth to display differing rates of ice growth, with the overtopping process allowing faster accretion since the frazil crystals are then directly exposed to the cold air temperatures.

3.1. Methods

[23] The model is divided into kinematic and thermodynamic parts. The kinematic model begins from a known observation time and position (such as an ice station) and drives the observed position backward in time, using appropriate wind factors and turning angles, until the beginning of a formation event. Forcing data is extracted along this track. The thermodynamic model then grows ice forward from this event time, using the extracted data to

force an energy balance model. Six-hourly time steps are used to grow (1) a congelation ice cover, in the absence of any oceanic turbulence and (2) frazil ice at a "free surface"; i.e., ice is removed as it forms, in the same manner as for polynya ice production. This represents the maximum possible ice production rate for a given forcing. We expect the rate of ice production in the pancake cycle to lie between these limits.

3.1.1. Data Assimilation

[24] Forcing fields were taken from merged in situ and model data: *Polarstern* meteorological data, transferred to the standard levels from sensor heights, are used while the ship occupied the main study area (days 106.5–110.0); ECMWF analysis data are used at other times. Parameters used are sea-level atmospheric pressure, wind at 10 m height, 2-m air temperature, 2-m dewpoint temperature (when using model data), relative humidity (when using ship data), and cloud cover fraction. When in situ data are used, these are taken as representative of the entire (relatively small) survey area. Though not ideal, the errors resulting from this approach are considerably smaller than the discrepancy between ECMWF and in situ measurements during this period, discussed below.

[25] Comparisons of in situ and model data show that the ECMWF model significantly underrepresents the severity of low air temperature events, a tendency also seen in previous comparisons [*Markus et al.*, 1998; *Vihma et al.*, 2002] and attributed to overestimation of the cloud cover fraction [*Vihma et al.*, 2002]. This is unfortunate, since thermodynamic growth models are particularly sensitive to air temperature variations. To increase the validity of the ice growth model during purely model-forced periods, we therefore calculate a T_{model} to $T_{\text{in situ}}$ relation, shown as a scatterplot in Figure 4. In situ air temperatures above -5°C are generally higher than modeled ($T_{\text{in situ}} = 0.42T_{\text{model}} - 1.08$), while temperatures lower than -8°C are fitted with a considerable offset ($T_{\text{in situ}} = 1.08T_{\text{model}} - 3.07$). Modeled values between -8°C and -5°C bear little consistent relation to in situ measurements, and we fit these values using a line of continuity between the two outer ranges ($T_{\text{in situ}} = 2.83T_{\text{model}} + 10.24$). The correction was tested against in situ data and gave a significant improvement, more than halving the difference between in-situ-forced and model-forced ice thicknesses.

[26] The effect of the correction on the ECMWF 2 m temperature time series is illustrated in Figure 5a. High temperatures between the ice growth events are slightly elevated and the severity of the low-temperature events is greatly enhanced. The ship data of event 2 are far more closely tracked by the corrected forcing. Buoy data, from day 111 (April 20), are also better followed though with variable success. The increased variability of the buoy data, swinging rapidly between extremes of temperature as the wind direction changes from an off-ocean to an off-ice direction, is clearly demonstrated and is poorly tracked by the model. The corrected forcing is taken in preference to the "raw" model data, though we are aware of the empirical nature of this correction and continue to cite uncorrected forcing results throughout, in addition to the corrected figures.

[27] In situ wind measurements also demonstrate a variable degree of correspondence to the ECMWF analysis, as shown in Figure 5b. The model performed well while the ship occupied the experimental area, but poorly while the buoys were close to the ice edge (days 111–120). This was likely due to local effects arising from the pinch-out of the bay and the thermal contrasts between ice and ocean there. Close agreement was reestablished once the bay closed and the buoys moved away from the edge, after day 120. The ship and buoy air pressure measurements were transmitted to the global telecommunication system (GTS) and used by the ECMWF model. Modeled winds are therefore not independent of the in situ measurements.

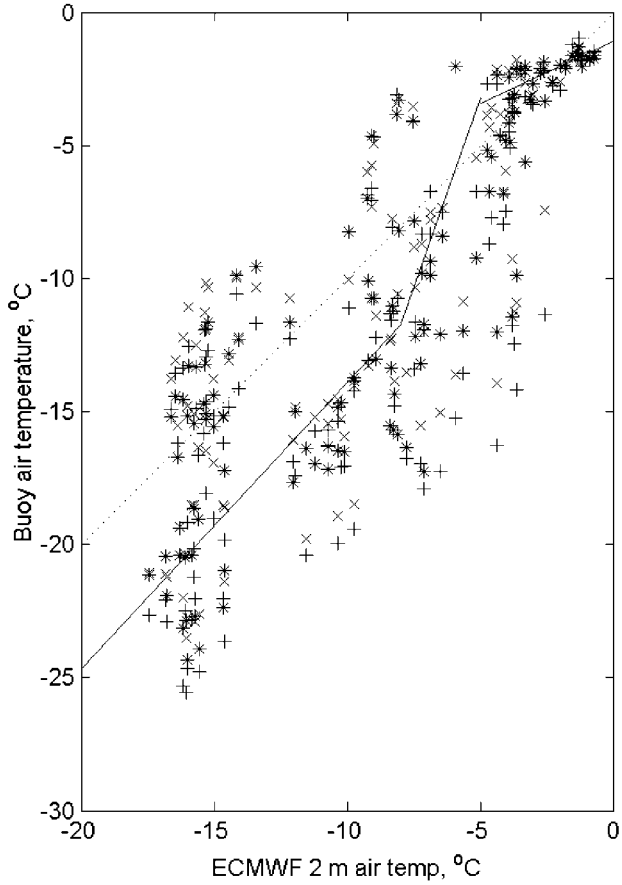

Figure 4. In situ air temperatures plotted against ECMWF 2-m temperature analysis, from day 111 (April 20) to day 140 (May 19). Symbols indicate results taken from three outer ice edge buoys, released at stations 0, 1, and 4, with the ECMWF forcing extracted along their track. The difficult nature of finding an empirical correction is clear. The three-piece line indicated was used to relate the two temperatures, and this succeeded in reducing the error by more than 50% between congelation ice produced using in situ forcing and that produced with model forcing. The dotted line indicates the ideal correspondence between the two parameters.

[28] Downwelling shortwave (SW) radiation was taken from shipborne measurements during the experiment and calculated analytically from the sun position at other times [*Cavalieri and Martin*, 1994]. Clear-sky transmittance was

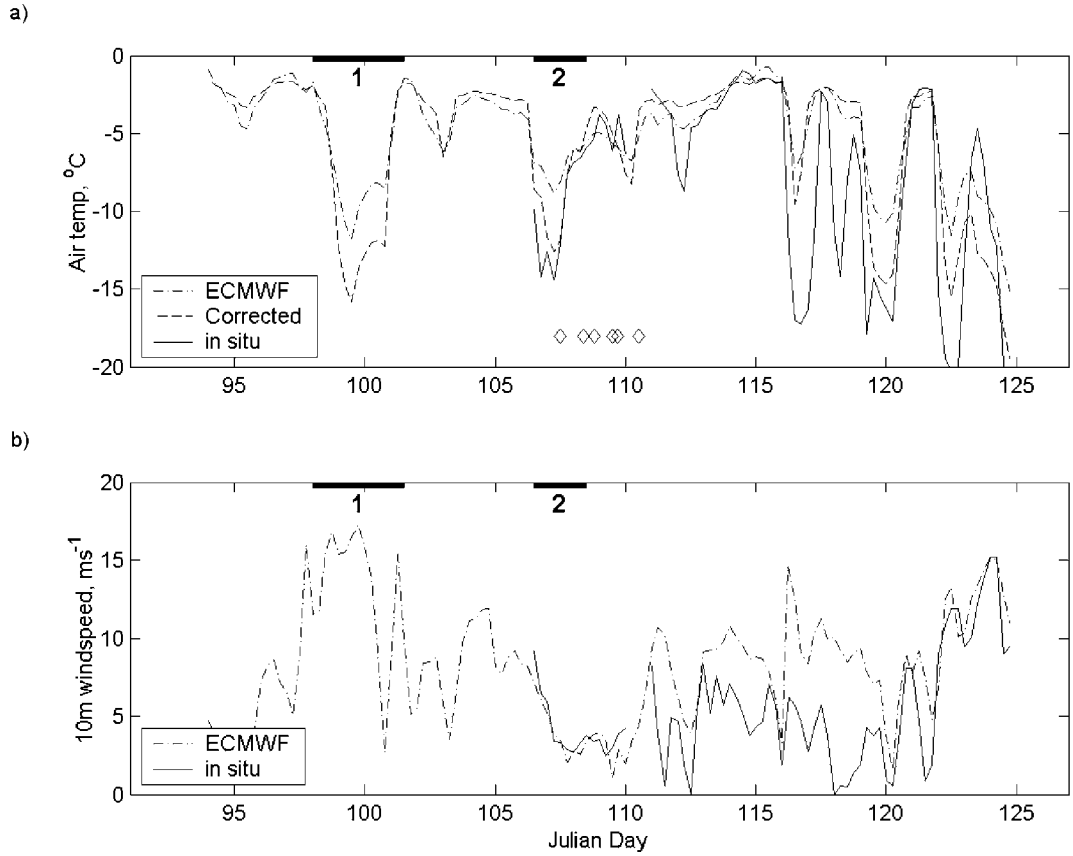

Figure 5. ECMWF analysis (a) 2-m air temperature and (b) 10-m wind speed compared to in situ measurements. Corrected air temperatures, using the regression shown in Figure 4, are also plotted (dashed line). The durations of the ice formation events are indicated as solid lines on the upper bound of each graph. Timing of the ice stations is indicated by the diamond symbols in the upper graph.

calculated using a parameterization developed for polar regions [*Shine*, 1984]. Cloud cover fraction was taken from the ECMWF "total cloud cover" analysis fields, using the *Laevestu* [1960] cloud correction factor. Relative humidity was taken from shipboard measurements or calculated from the ECMWF 2 m dewpoint temperature fields [*Rogers and Yau*, 1989], as appropriate.

3.1.2. Thermodynamic Model

[29] The heat fluxes present at the top surface of congelation ice are [*Maykut*, 1986],

$$(1-\alpha)Q_s - I_0 + Q_B - Q_{up} + Q_H + Q_E + Q_C = Q_{net}, \qquad (1)$$

where α is the albedo, Q_S is the downwelling SW radiation flux, I_0 is the SW radiation which penetrates the ice, Q_B is the downwelling longwave (LW) radiation flux from the air, Q_{up} is the upwelling LW radiation flux from the ice surface, Q_H is the sensible heat flux, Q_E is the latent heat flux, and Q_C is the conductive heat flux upward to the ice surface. Terms away from the surface are negative; those toward the surface are positive. The sum is zero if the ice surface is below freezing point, with the balance determined by the (unknown) ice surface temperature, T_0 [*Maykut*, 1986]. We first solve terms which do not depend on T_0 (Q_S, I_0, Q_B) and then iteratively solve equation (1) to give T_0 [*Eisen and Kottmeier*, 2000].

[30] The thin, young ice considered in the congelation model makes it unnecessary to use complex, snow-covered, multilayer ice models [*Rudels et al.*, 1999]. The snow-free assumption is reasonable since no significant snow layer was observed in the area during the experiment. We assume the ice can be approximated by a homogeneous conducting slab; though nonlinear profiles have been observed in Weddell Sea ice, these are ascribed to "drastic air temperature excursions" [*Eicken*, 1992] and are a transient feature for ice less than ~0.8 m thickness.

[31] The bottom surface of the ice is assumed to be at the freezing temperature of seawater ($T_f = -1.89$°C) for the measured mixed-layer salinity (34.35 psu, held constant). If the melting temperature of the ice (−0.6°C at an assumed constant salinity = 11 psu) is reached without balance being achieved, T_0 is set to this value [*Simonsen and Haugan*, 1996] and the resulting positive heat flux is used to melt ice at the top surface. In fact, the calculated surface temperature never rose to this level during the period of interest.

[32] The turbulent heat coefficient used in sensible and latent heat calculations [e.g., *Budillon et al.*, 2000; *Large and Pond*, 1982; *Maykut*, 1978] is estimated from the Appendix of *Kondo* [1975], using a lookup table containing seven classes of surface-atmosphere temperature difference and six classes of windspeed. Albedo is calculated as that of snow-free thin-ice [*Weller*, 1972]. Latent heat of sublima-

tion (over ice) is taken as a constant (2837 kJ kg^{-1}). Latent heat of vaporization (over water) is varied with surface temperature, as given by *Rogers and Yau* [1989]. Moist air density, vapor pressure, specific humidity and mixing ratio equations are taken from *Rogers and Yau* [1989].

[33] At the bottom surface of the ice the situation is simpler, with just the ocean-ice heat flux (F_w, positive from the ocean to the ice) and the conductive heat flux from the ocean to the ice (Q_{CB}, negative away from the ice-ocean interface) contributing. No balance occurs, and the net heat flux at the bottom surface of the ice either grows or melts ice depending on its sign. The rate of change in ice thickness at the bottom surface is then given by [*Maykut and Perovich*, 1987]

$$\frac{\partial h}{\partial t} = -\frac{1}{\rho_i L}(Q_{CB} + F_w), \tag{2}$$

where h is the ice thickness (m), ρ_i is the density of ice (taken as 920 kg m^{-3}), and L is the latent heat of fusion, 295.8 kJ kg^{-1}, equivalent to ice containing 10% brine volume [*Haarpaintner et al.*, 2001]. Estimates of F_w in the study area range from 5 W m^{-2} [*Lytle and Ackley*, 1996], through 27.4 W m^{-2} [*McPhee et al.*, 1999] to more than 40 W m^{-2} [*Gordon and Huber*, 1990]. We use an intermediate value of 25 W m^{-2} [*Martinson*, 1990; *Martinson and Iannuzzi*, 1998], since the relatively thick pycnocline at the beginning of winter will reduce the heat flux to well below its maximum value. Q_{CB} is given by

$$Q_{CB} = \frac{\kappa_i}{h}(T_0 - T_f), \tag{3}$$

where κ_i is the thermal conductivity of the ice, which is calculated according to *Maykut* [1978]. We hold the ice salinity constant at 11 psu in this parameterization, since the salinity evolution of pancake ice is currently poorly constrained. Ice temperature is assumed to be the mean of the surface and base temperatures.

[34] Frazil ice growth was accomplished using a similar scheme, omitting the conduction terms and setting $T_0 = T_f$. The equation, balanced by the ice formation and taking heat gain by the ocean as positive, becomes

$$Q_H + Q_E + Q_B - Q_{up} + Q_S = -\rho_i L \frac{\partial h}{\partial t}, \tag{4}$$

where $\frac{\partial h}{\partial t}$ is the frazil formation rate, expressed as an equivalent solid ice thickness. L is the latent heat of fusion, taken as that for ice crystals suspended in freezing seawater at constant temperature = 234.14 kJ kg^{-1} [*Haarpaintner et al.*, 2001]. The frazil ice density ρ_i is taken as 950 kg m^{-3}, as commonly used in the literature [*Markus et al.*, 1998; *Martin and Kaufmann*, 1981].

[35] For both ice types, the resulting ice growth rate is multiplied by the time step and added to the existing ice thickness. The model then repeats the process for all time steps until the end of the period of interest. Thickness is output as "equivalent solid ice." For direct comparison with the model, the observed ice thickness is converted to its solid ice equivalent. The experiment determined that approximately 30% of the pancake volume was porous space, and we accordingly reduce observed pancake layer thicknesses, multiplying by the volume concentration of ice (V_p = 0.7) to obtain their solid ice equivalent. Volume concentration of the frazil slicks (V_f) was observed to be 0.4 [*Doble et al.*, 2000]. This is slightly higher than figures quoted in the literature, for example, 0.3 [*Bauer and Martin*, 1983], reflecting the low levels of turbulence before sampling which allowed the slick to become more consolidated than would be the case during active formation events. Total equivalent ice production must also account for the area fraction of each ice type (f_p, f_f) to conserve ice volume. The final observed solid ice thickness per unit area sea surface is therefore

$$H_{obs} = h_p V_p f_p + h_f V_f f_f, \tag{5}$$

where h_p and h_f are the observed pancake and frazil slick thicknesses, respectively.

3.1.3. Kinematic Model

[36] Wind factors were derived using a two-parameter regression method [*Vihma et al.*, 1996] taking drift data from the buoys released at each station. Values used were

Wind factor = 0.029

Turning angle = 13°(to the left)

Residual current, $u-$component = -0.045 ms^{-1}

Residual current, $v-$component = $+0.023$ ms^{-1}

Validation tests using coincident buoy tracks over a 10-day timescale gave RMS position errors (between actual buoy and backward-modeled tracks at the end of the simulation) of approximately 2.5 km. Modeled advection over the period of interest displaced the ice position by only ~40 km. This is of the same order as an ECMWF model grid cell (1.125° × 1.125° or 125 × 41 km at this latitude) and gives confidence in the forcing extracted along the track.

3.2. Results

3.2.1. Determination of Layer Growth Periods

[37] Running the model over the period prior to the experiment identified two distinct and dominant events of ice production, separated by essentially zero growth/melt periods. Modeled fluxes for congelation and free-surface frazil ice growth are shown in Figure 6. The graphs show the fluxes at the backtracked location of station 5 and use the corrected forcing data. Turbulent fluxes dominate the energy balance for both types of ice growth, with the sensible heat flux being approximately double the latent heat contribution. The conductive heat flux through the top surface of the congelation ice, though larger in magnitude than the turbulent flux (up to 290 W m^{-2}), is balanced by an almost equal and opposite sign flux across the ocean-ice interface, and is not shown. Net longwave and shortwave fluxes are small in comparison. The onset of these events is essentially coincident for all six main area stations.

[38] Modeled frazil production indicates positive net fluxes only for brief periods around noon between the events (Figure 6b). These occur in phase with the downwelling SW radiation when the relatively high air temperatures and low winds result in very small heat loss by the

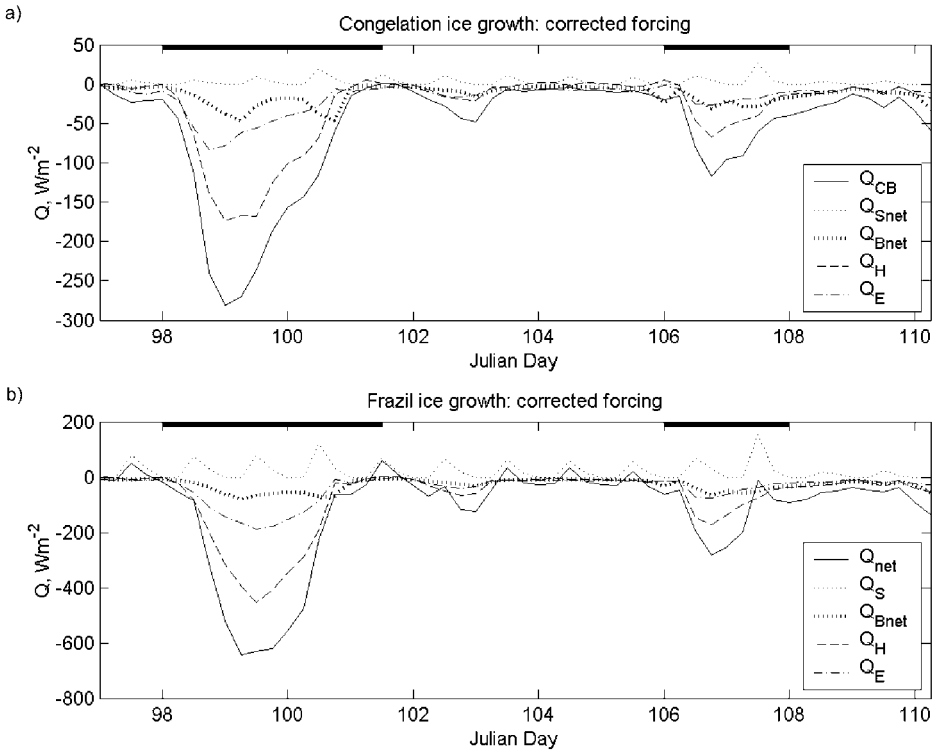

Figure 6. Modeled heat fluxes using corrected forcing. Fluxes for (a) congelation ice growth and (b) free-surface frazil growth are shown, both at the back-tracked location of station 5. The durations of the ice formation events are indicated as solid lines on the upper bound of each graph. The distinct ice growth events are clearly shown, with turbulent heat fluxes dominating.

ocean. The conductive heat flux from the ocean to the ice (Q_{CB}) is only slightly negative (~ -10 W m^{-2}) between events and is smaller in magnitude than the oceanic heat flux F_w. Melt therefore occurs on the bottom surface of the modeled congelation ice growth, reducing ice thickness by $\sim$1 cm between growth events.

[39] Each event is taken to have resulted in the growth of one pancake layer. Type A pancakes were observed to have grown entirely during event 2. Modeled growth of these was therefore begun at the start of event 2 (day 106) and stopped at the observation time. We assume that the top layers of two-layer types also formed during this latter event. Growth of this layer was begun at the end of event 1 (day 101.5), however, since a platform for its growth already existed at this time and the presence of type B pancakes suggested that top-layer growth proceeded soon after the platforms were grown. Bottom layers are taken to have formed during event 1, and all bottom layer growth was therefore begun at the start of event 1 and halted at the end of that event, on day 101.5. This was done since the top layer of frazil-grown ice is porous to seawater, resulting in the upper and lower surfaces of the submerged platform being at the same temperature. We have seen that the greatest heat fluxes for congelation ice growth are conductive and sensible and both of these will be zero for the submerged ice platform.

3.2.2. Event 2

[40] The simulation was first run for the most recent growth period, for all main-area stations. The long-scale station 6 was omitted from these calculations since a third frazil formation event was underway there before observations were taken. Figure 7a shows the modeled solid ice thickness for congelation and free-surface frazil growth, with the observed mean layer thicknesses at each station, corrected for volume concentration and area according to equation (5), marked as solid symbols. Error bars indicate the standard deviation of the observed ice layer thickness. Corrected modeled thickness is less than the "raw" figure due to the 5 days of relatively high air temperatures after event 1, and the resulting positive temperature correction. Event 2 itself is forced using in situ data, which is identical for corrected and uncorrected data.

[41] The observed type A pancakes at three stations (1, 3, and 4) have equivalent solid ice thicknesses (3.5 ± 0.6 cm, 5.5 cm, 5.2 ± 0.3 cm, respectively) significantly less than even the congelation ice growth value. Mean thicknesses of the top layers lie significantly above the congelation ice equivalent, however, with the upper range of observed values reaching approximately double the congelation ice figure or half the maximum physically possible value.

3.2.3. Event 1

[42] Results for bottom-layer growth are shown in Figure 7b. Corrected modeled growth in this case is higher than the uncorrected results, due to significantly colder corrected air temperatures during the formation event. The area fraction for pancakes grown during this event is assumed equal to that seen at the end of event 2, neglecting type A pancake formation in the interstices and the slightly

larger diameter of the top layers. We do not include any contribution from the frazil ice remaining in the interstices between pancakes since it could not be directly measured. Thickness for type D bottom layers is not adjusted for porosity (since they are columnar, not granular ice) or area, since they formed in large areas of calm water identical to that considered for the modeled congelation ice growth.

[43] Observed thickness of type D platforms is much higher than modeled growth, implying that these were formed earlier and advected into the area. It would require 250 degree-days to grow the mean 33 cm columnar ice layer observed at station 0: both events combined constitute only 44 degree-days, equivalent to 12-cm ice growth.

[44] The type B lower layers grown during this event are analogous to the type A pancakes seen after event 2. They demonstrate similar low growth rates, with their equivalent solid ice thickness plotting well below that of the modeled congelation ice at stations 0, 3, and 5, and support the surprisingly slow type A growth seen during event 2.

3.2.4. Combined Growth

[45] The disparate rates of formation ascribed to the two processes combine to produce a two-layer pancake whose overall rate of thickness increase must lie between that of each layer. This "overall growth rate" is perhaps the most important parameter, since it is the overall thickness of the pancake which determines the fluxes across the ocean-air interface and the mass of salt rejected to the mixed layer.

[46] We therefore model growth beginning at the start of event 1 and continuing to the observation time. Results are presented in Figure 7c. Equivalent thicknesses are presented only for type B pancakes, since they are the only two-layer, frazil-grown pancakes considered here. Results match the congelation ice equivalents closely, though actual pancake thickness (not corrected for area) is approximately double the congelation equivalent.

3.2.5. Sensitivity Tests

[47] The model's response to variations in forcing parameters was tested. Results are summarized in Table 3. The table shows modeled growth at the backtracked location of station 3, beginning at the start of event 1 and continuing until the observation time.

[48] Oceanic heat flux influences ice production by approximately half the proportion of the change in that parameter (e.g., a reduction of 60% in F_w increases congelation ice thickness by 30%). A fixed cloud cover fraction shows the model to be relatively insensitive to this parameter, since cloud has two opposing effects: cutting down incident solar radiation but increasing downwelling longwave radiation through increased effective emissivity of the air. Given the relatively advanced season and short daylight hours, it is the longwave effect which dominates, increasing ice growth with reduced cloud cover. Relative humidity affects the latent heat flux, which has a small contribution to the overall flux balance and is reflected in the minor response of the model.

[49] The model is considerably more sensitive to changes in air temperature and windspeed, with the magnitude of the

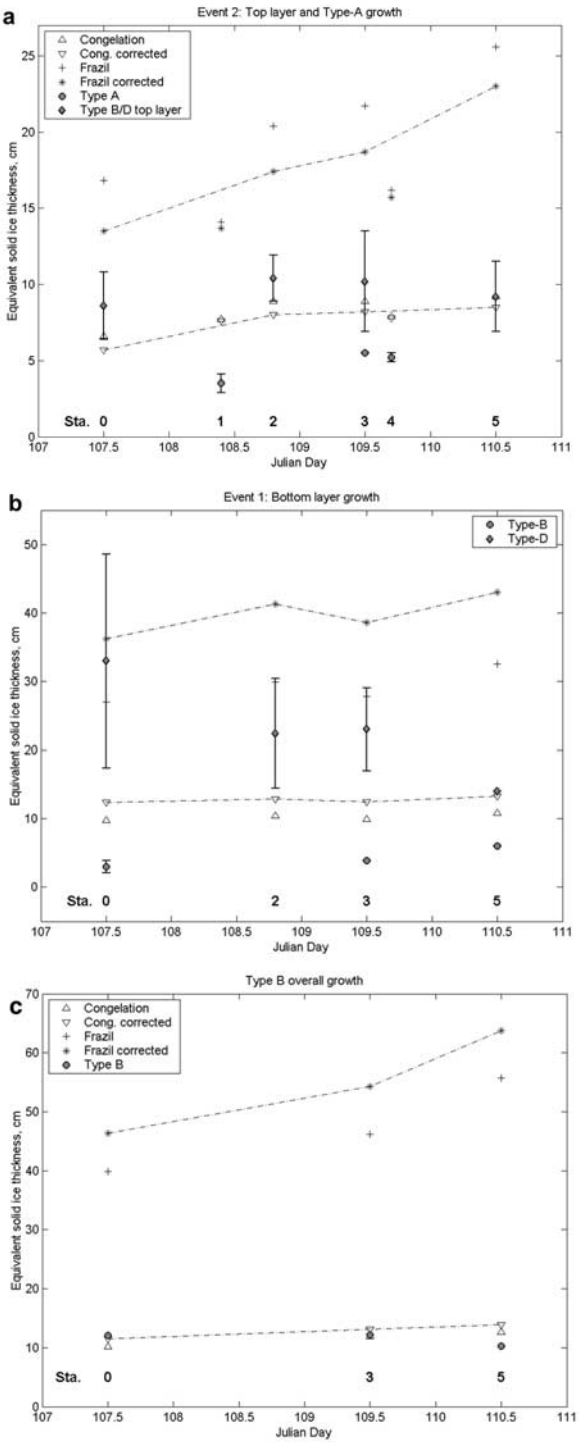

Figure 7. (opposite) Observed ice thickness at each ice station plotted together with the corresponding modeled thickness for congelation and frazil ice growth at that observation time. The three graphs show (a) top layers and single layer pancakes, formed during event 2; (b) lower layers, formed during event 1; and (c) overall pancake growth across both events. Mean equivalent layer thicknesses are plotted, with error bars indicating their standard deviation. The modeled congelation and frazil ice growth which would have occurred under the same forcing is indicated both for "raw" and corrected forcing. Corrected forcing results are also linked by dash-dotted lines. Station numbers (Sta.) corresponding to each observation are shown above the x axis.

Table 3. Sensitivity of the Model to Changes in Forcing Parameters[a]

Parameter	Variation	h_c Error,%	h_f Error,%
Cloud fraction, *Tcc*	0.6−var−1	+24/−3	+31/−3
Relative humidity, *Rh*	80−var−95	+3/−1	+5/−8
Oceanic heat flux, F_w	10−25−40	+30/−26	–
Air temperature, T_a	±1°C	−21/+19	−25/+25
Wind speed, V_{10}	±2 m s^{-1}	+7/−12	+19/−20

[a]Figures in the variation column show the minimum-normal-maximum values through which the parameter was varied, if held constant, or the offset from the varying value Changes are expressed as percentages of the final uncorrected ice thickness for congelation ice (h_c) and frazil ice (h_f) growth modes. Growth was modeled at the backtracked location of station 3, beginning at the start of event 1 and continuing to the observation time.

response being broadly equivalent to the percentage change in the parameter. ECMWF windspeeds have been found to be accurate, but the failings in modeled air temperatures already discussed are of more concern. The model's sensitivity is unfortunately an unavoidable aspect of the physics involved and is reflected in the large separation between corrected and uncorrected thickness values during event 1. This should be taken into consideration when considering modeled thickness results.

3.3. Discussion

[50] The equivalent thickness of the type A and lower layer type B pancakes is unexpectedly low, given previous conjecture about pancake formation rates [*Hopkins and Shen*, 2001; *Wadhams et al.*, 1987]. The consistency between types indicates that similar processes are responsible for the formation of these layers and gives confidence in the correspondence between layers and events.

[51] A clear disparity in ice growth rates exists between type A pancakes and the type B/D top layers, however. The disparity becomes more marked if we consider that top-layer growth occurred with the existing platforms (from event 1) significantly reducing the area of sea surface available for ice production during the second event. These bottom layers must have occupied a similar area fraction at the beginning of event 2 to that seen at its end, implying that only ~40% of the total area was available for frazil production during this event. This suggests that the observed equivalent solid ice thickness should be increased accordingly.

[52] An opposing consideration is the fate of the frazil fraction remaining at the end of event 1. The transient nature of the positive heat flux episodes indicates that significant melt did not occur and the lack of granular ice underneath the type D congelation ice suggests that the frazil did not accrete below the platforms in the five days between events. The frazil layer was also never observed to extend deeper than the pancakes during ROV flights, though these were conducted in conditions of low turbulence. It must therefore either have remained as frazil ice, increasing the thickness of the frazil slick observed at the end of event 2, or accreted to the top surface of the platforms, adding to the perceived top-layer production during event 2. Either process would contribute additional volume to the ice formed during event 2 and require a downward correction in the equivalent solid ice thickness due to that event.

[53] The balance of these opposing corrections is unknown in the absence of comprehensive field or ice tank observations over similar periods. It is probable that the "available surface" correction will dominate, since the contribution from remaining frazil is relatively small as it is reduced by $V_f = 0.4$ and the smaller area fraction of this ice type. The true equivalent top-layer thickness is therefore likely to be higher than Figure 7a indicates. Consideration of the overall growth removes the need for the effective area and event 1 frazil corrections and gives a more reliable comparison to congelation and frazil equivalent thickness.

4. General Discussion

[54] The model identifies two distinct forcing events and indicates that two, widely differing, rates of ice accretion occurred during the second event. The pancake morphologies and their salinities also support the assumption that the lower rate process represents the classical pancake growth mechanism and the higher rate process is due to top-layer growth.

[55] It seems unlikely that classical pancake growth proceeds at a rate below that of congelation ice, however, and this unexpectedly low rate may arise from errors induced by the many assumptions required. The period between events, when ocean-atmosphere fluxes are almost zero and the oceanic heat flux becomes significant, is one possible source of this error. Higher air temperatures than the ECMWF temperature data suggest, or higher values of oceanic heat flux than assumed might lead to significant melting of the frazil or pancake ice during this finely balanced period. If melt occurs, ice production during the first event would be significantly underrepresented. The sea surface temperature would also become elevated to the north of the ice edge, requiring the reestablishment of a freezing surface layer before frazil and pancake production could begin during the second event. The same error in forcing would thus lead to a consistent error in pancake growth rates for the classical mechanism, as seen. A similar effect would also apply to upper layer growth, however, since frazil production during this process will also be delayed until an appropriate sea surface temperature is regained. The disparity between the formation rates arising from the two mechanisms therefore remains a robust conclusion.

[56] The disparity in rates is understandable, since dumping frazil above the waterline, where it is directly in contact with the cold air temperatures, is a more efficient method of accretion than attempting to sinter frazil to the underside of a pancake at close to the freezing temperature of seawater. Contrary to the growth modeled by *Hopkins and Shen* [2001], solid pancake rafting can be excluded as the mechanism for the observed two-layer structure since (1) little rafting was observed outside the compaction zone caused by the ship's passage; (2) salinity and porosity contrasts would be reversed and reduced for rafted layers of similar age; and (3) the wedge-shaped top layers observed have no obvious cause under the rafting mechanism.

[57] The clear demarcation of layers in the type D pancakes was instrumental in alerting the authors to the less striking type B and type C forms. We note that the type A pancakes sampled here were strong compared with those seen in the Odden in 1997; none were broken during removal from the lifter, even when they were only 5 cm thick. This arises due to the lower air temperature events here compared to the Odden area, and suggests that only a

short time need elapse before frazil-rafting can begin. The overtopping mechanism may therefore be extremely common in the Antarctic, though the absence of the obvious type D pancakes has allowed the two layer types to remain undetected until now. Type D pancakes may be unusual and confined to an ''oscillating'' ice edge, which allows the juxtaposition of low freeboard congelation ice and frazil growth. The disparity in accretion rates between the two mechanisms suggests that top-layer growth will dominate pancake ice accretion where it occurs.

[58] The low overall equivalent thicknesses (Figure 7c) are unexpected, given previous speculation about pancake formation rates. It should be borne in mind, however, that the pancakes are rather thin in comparison with a typical final pancake thickness of ~50 cm. Further thickness increases will be dominated by the top growth process, increasing the overall rate toward that of the faster mechanism. Equivalent congelation ice growth is also greatly reduced once the ice cover begins to thicken to these levels, thus pancake and congelation ice growth rates can be expected to diverge more significantly in the latter stages of the pancakes' evolution.

[59] The existence of top-layer growth naturally leads to a search for how frazil in the water column can overcome the freeboard of the existing layer to be deposited on top. Pancake motion in the wavefield, as the pancake tilts in less than perfect alignment with the wave surface, can scoop the frazil suspension onto the top surface. We might expect this to occur preferentially on the up wave side of the pancake, since the horizontal component of the orbital wave motion can then wash the suspension onto the surface. This gives rise to the wedge-shaped top layers seen in the field and illustrated in Figure 2 for type C and type D. Indeed, type C and type D pancakes were never encountered with a constant thickness upper layer.

[60] ''Squirting'' and ''pumping'' of the frazil suspension between cakes, building the familiar rims as the pancakes open and close in the wave field, also occurs. The poorly consolidated rims can then be washed across the surface of the pancake during large amplitude excursions, adding a layer of frazil and building the platform upward. Large-amplitude waves result in the pancakes being ''completely washed over by water'' [*Wadhams and Wilkinson*, 1999], though this might result in unconsolidated frazil being washed back into the water rather than enhancing top growth. Constant addition of frazil to the outside of the rim during collisions itself implies upward growth of the pancake, since the pancake platform cannot support the increasing weight of the rim without being pushed underwater, again allowing the rim to be washed across its surface. Indeed, once considered, it is hard to see how top-layer growth cannot occur.

[61] Tank experiments suggest that the amplitude of swell required to produce top-layer growth is rather low. In the latter stages of wave-influenced ice growth in the tank, the ice cover consisted of rigid plates separated by only thin cracks of open water allowing flexure. The top surfaces remained wet under these conditions and top-layer growth continued, though at a much reduced rate. The limit to top-layer growth is the diameter of the lower layer, since the pancake is unstable in the water once this figure is approached. Pancakes nearing this limit were seen at station 3, with pancakes 15 and 21 (both type D) being almost spherical in form. Pancake building will end in any case if the wave field is removed or when there is no more open water.

[62] The lack of two layer pancakes seen in the Odden may be due to the surface melt conditions common in that region. Surface melt flushing would tend to remove the signature of top-layer growth in pancakes which have experienced higher air temperatures for any length of time. A cruise to the region in March 2001 encountered pancakes which had not experienced a melt flushing event, however (M. Doble, unpublished data, 2001). These consistently displayed similar salinity profiles to the Weddell Sea pancakes, suggesting that the top growth process may dominate there too.

5. Conclusions

[63] We have presented the first well-constrained pancake ice growth rates in the field and established a top-layer growth mechanism in addition to the familiar bottom-accretion process. Support for this new mechanism is set out using the observed morphologies, salinities, and temperature profiles, as well as direct observations during ice tank experiments.

[64] Modeled ice growth demonstrates disparate growth rates for each mechanism and is expressed as an equivalent solid ice thickness per unit sea surface area, corrected for volume concentration and area fraction of frazil and pancake ice. The initial growth of pancakes, whether the classic single-layer type A or the lower layer of type B, is demonstrated to be rather slow, though it is unlikely to actually be slower than the limiting case of congelation ice growth. Top-layer growth produces ice significantly faster, though the exact rate is difficult to determine, since the free surface available for growth is reduced by the existing platforms and the contribution from any frazil slick remaining from the lower layer growth is unknown. Neglecting these effects, we find that top-layer ice production proceeds at up to double the congelation ice equivalent and half that which would result from free-surface frazil growth.

[65] Overall ice production by these combined processes is similar to the equivalent congelation-grown volume while the pancakes are less than ~20 cm thick. This equivalence is due to the slow initial pancake formation by bottom accretion, which contributes an appreciable part of the total thickness at this early stage. Subsequent growth of the pancakes will be substantially faster, since the relatively rapid top-layer growth will dominate while the equivalent congelation ice growth rate drops rapidly with increasing thickness. Given the disparity in growth rates, it is further suggested that the top-growth mechanism dominates thickness increase once the growing platform becomes consolidated enough to support the overtopping process. Pancakes thicker than 10 cm appear likely to be dominantly type B composites rather than bottom-accreted forms.

[66] Conceptual models which simulate pancake ice growth currently increase pancake thickness by either extending the freezing front downward as additional buoyancy from bottom-accreted frazil pushes the pancake upward, or by rafting of solid pancakes [*Shen et al.*, 2001]. Our results suggest that the new top-layer growth process must be parameterized if a realistic thickness is to be

simulated. By extension, the process and its resulting rate of ice growth must be included in any simulation of the thickening of a wave-influenced ice cover if the evolution of heat and salt exchange between ocean and atmosphere in global models is to be correctly followed.

[67] **Acknowledgments.** We would like to thank Captain Jürgen Kiel and the *Polarstern* crew for their unflagging help during the field experiment, Leif Toudal (Danish Technical University) for supplying his Java browser and satellite ice images onboard and afterward, Andreas Starmans (AWI) and his team for the ROV deployments, Gerhard Dieckmann (AWI) for the loan of his ice sampling basket, and Oli Peppe, Duncan Mercer, and David Meldrum (Dunstaffnage Marine Laboratory) for their efforts far beyond the call of duty. We would also like to thank the anonymous referees and Victoria Turner for their comments and suggestions, which greatly improved the manuscript. Work was supported by the Natural Environment Research Council grant GR3/12952.

References

Armstrong, T., B. Roberts, and C. Swithinbank, *Illustrated Glossary of Snow and Ice*, 60 pp., Scott Polar Res. Inst., Cambridge, England, 1973.

Bauer, J., and S. Martin, A model of grease ice growth in small leads, *J. Geophys. Res.*, *88*(C5), 2912–2925, 1983.

Budillon, G., G. Fusco, and G. Spezie, A study of surface heat fluxes in the Ross Sea (Antarctica), *Antarct. Sci.*, *12*(2), 243–254, 2000.

Cavalieri, D. J., and S. Martin, The contribution of Alaskan, Siberian and Canadian coastal polynyas to the cold halocline layer of the Arctic Ocean, *J. Geophys. Res.*, *99*(C9), 18,343–18,362, 1994.

Clarke, D. B., and S. F. Ackley, Sea ice structure and biological activity in the Antarctic marginal ice zone, *J. Geophys. Res.*, *89*(C2), 2087–2095, 1984.

Cox, G. F. N., and W. F. Weeks, Numerical simulations of the profile properties of undeformed first-year sea ice during the growth season, *J. Geophys. Res.*, *93*(C10), 12,449–12,460, 1988.

Doble, M. J., M. D. Coon, and O. Peppe, Cruise report: F/S Polarstern ANT-XVII/3, report, Scott Polar Res. Inst., Cambridge, England, 2000.

Doble, M., M. Coon, and O. Peppe, Study of the winter Antarctic marginal ice zone, *Ber. Polar Meeresforschung*, *402*, 158–161, 2001.

Eicken, H., Salinity profiles of Antarctic sea ice: Field data and model results, *J. Geophys. Res.*, *97*(C10), 15,545–15,557, 1992.

Eisen, O., and C. Kottmeier, On the importance of leads in sea ice to the energy balance and ice formation in the Weddell Sea, *J. Geophys. Res.*, *105*(C6), 14,045–14,060, 2000.

European Centre for Medium-range Weather Forecasts, The description of the ECMWF/WCRP Level III-A Global Atmospheric Data Archive, Reading, England, 1997.

Gloersen, P., W. J. Campbell, D. J. Cavalieri, J. C. Comiso, C. L. Parkinson, and J. Zwally, *Arctic and Antarctic Sea Ice, 1978–1987: Satellite Passive-Microwave Observations and Analysis*, 290 pp., NASA/Goddard Space Flight Cent., Greenbelt, Md., 1992.

Gordon, A. L., and B. A. Huber, Southern Ocean winter mixed layer, *J. Geophys. Res.*, *95*(C7), 11,655–11,672, 1990.

Gow, A. J., S. F. Ackley, K. R. Buck, and K. M. Golden, Physical and structural characteristics of Weddell Sea pack ice, report, Cold Reg. Res. and Eng. Lab., Hanover, N. H., 1987.

Haarpaintner, J., J.-C. Gascard, and P. M. Haugen, Ice production and brine formation in Storfjorden, Svalbard, *J. Geophys. Res.*, *106*(C7), 14,001–14,013, 2001.

Hanley, T. O. D., and G. Tsang, Formation and properties of frazil in saline water, *Cold Reg. Sci. Technol.*, *8*, 209–221, 1984.

Hopkins, M. A., and H. H. Shen, Simulation of pancake ice dynamics in a wave field, *Ann. Glaciol.*, *33*, 355–360, 2001.

Kondo, J., Air-sea bulk transfer coefficients in diabatic conditions, *Boundary Layer Meteorol.*, *9*, 91–112, 1975.

Laevestu, T., Factors affecting the temperature of the surface layer of the sea, *Comment. Phys. Math.*, *25*, 1–36, 1960.

Lange, M. A., and H. Eicken, Textural characteristics of sea ice and the major mechanisms of ice growth in the Weddell Sea, *Ann. Glaciol.*, *15*, 210–215, 1991.

Lange, M. A., S. F. Ackley, P. Wadhams, G. S. Dieckmann, and H. Eicken, Development of sea ice in the Weddell Sea, *Ann. Glaciol.*, *12*, 92–96, 1989.

Lange, M. A., P. Schlosser, S. F. Ackley, P. Wadhams, and G. S. Dieckmann, ^{18}O concentrations in sea ice of the Weddell Sea, Antarctica, *J. Glaciol.*, *36*(124), 315–323, 1990.

Large, W. G., and S. Pond, Sensible and latent heat flux measurements over the ocean, *J. Phys. Oceanogr.*, *12*, 464–482, 1982.

Lytle, V. I., and S. F. Ackley, Heat flux through sea ice in the western Weddell Sea: Convective and conductive transfer processes, *J. Geophys. Res.*, *101*(C4), 8853–8868, 1996.

Markus, T., C. Kottmeier, and E. Fahrbach, Ice formation in coastal polynyas in the Weddell Sea and their impact on oceanic salinity, in *Antarctic Sea Ice: Physical Processes, Interactions and Variability*, *Antarct. Res. Ser.*, vol. 74, edited by M. O. Jeffries, pp. 273–292, AGU, Washington, D. C., 1998.

Martin, S., Frazil ice in rivers and oceans, *Ann. Rev. Fluid Mech.*, *13*, 379–397, 1981.

Martin, S., and P. Kaufmann, A field and laboratory study of wave damping by grease ice, *J. Glaciol.*, *27*(96), 283–313, 1981.

Martinson, D. G., Evolution of the Southern Ocean winter mixed layer and sea ice: Open ocean deepwater formation and ventilation, *J. Geophys. Res.*, *95*(C7), 11,641–11,654, 1990.

Martinson, D. G., and R. A. Iannuzzi, Antarctic ice-ocean interaction: Implications from bulk property distributions in the Weddell Gyre, in *Antarctic Sea Ice: Physical Processes, Interactions and Variability*, *Antarct. Res. Ser.*, vol. 74, edited by M. O. Jeffries, pp. 243–272, AGU, Washington, D. C., 1998.

Maykut, G. A., Energy exchange over young sea ice in the central Arctic, *J. Geophys. Res.*, *83*(C7), 3646–3654, 1978.

Maykut, G. A., The surface heat and mass balance, in *The Geophysics of Sea Ice*, edited by N. Untersteiner, pp. 395–463, Plenum, New York, 1986.

Maykut, G. A., and D. K. Perovich, The role of shortwave radiation in the summer decay of a sea ice cover, *J. Geophys. Res.*, *92*(C7), 7032–7044, 1987.

McPhee, M., C. Kottmeier, and J. H. Morison, Oceanic heat flux in the central Weddell Sea during winter, *J. Phys. Oceanogr.*, *29*, 1166–1179, 1999.

Rogers, R. R., and M. K. Yau, *A Short Course in Cloud Physics*, 293 pp., Pergamon, New York, 1989.

Rudels, B., H. J. Friedrich, D. Hainbucher, and G. Lohmann, On the parameterisation of oceanic sensible heat loss to the atmosphere and to ice in an ice-covered mixed layer in winter, *Deep Sea Res.*, *46*(6–7), 1385–1426, 1999.

Shen, H. H., S. F. Ackley, and M. A. Hopkins, A conceptual model for pancake ice formation in a wave field, *Ann. Glaciol.*, *33*, 361–367, 2001.

Shine, K. P., Parameterisation of shortwave flux over high albedo surfaces as a function of cloud thickness and surface albedo, *Q. J. R. Meteorol. Soc.*, *110*, 747–760, 1984.

Simonsen, K., and P. M. Haugan, Heat budgets of the Arctic Mediterranean and sea surface heat flux parameterizations for the Nordic Seas, *J. Geophys. Res.*, *101*(C3), 6553–6576, 1996.

Squire, V. A., The marginal ice zone, in *The Physics of Ice Covered Seas*, edited by M. Lepparanta, pp. 381–446, Univ. of Helsinki, Helsinki, 1998.

Thomas, D. N., and J. P. Wilkinson, European ARCTELAB large scale facility: Final report, INTERICE 3, Univ. of Wales, Bangor, Wales, 2001.

Tison, J.-L., and V. Verbeke, Chlorinity/salinity distribution patterns in experimental granular sea ice, *Ann. Glaciol.*, *33*, 13–20, 2001.

Ushio, S., and M. Wakatsuchi, A laboratory study on supercooling and frazil ice production processes in winter coastal polynyas, *J. Geophys. Res.*, *98*(C11), 20,321–20,328, 1993.

Vihma, T., J. Launiainen, and J. Uotila, Weddell Sea ice drift: Kinematics and wind forcing, *J. Geophys. Res.*, *101*(C8), 18,279–18,296, 1996.

Vihma, T., J. Uotila, B. Cheng, and J. Launiainen, Surface heat budget over the Weddell Sea: Buoy results and model comparisons, *J. Geophys. Res.*, *107*(C2), 3013, 10.1029/2000JC000372, 2002.

Wadhams, P., and J. P. Wilkinson, The physical properties of sea ice in the Odden ice tongue, *Deep Sea Res.*, *46*(6–7), 1275–1301, 1999.

Wadhams, P., M. A. Lange, and S. F. Ackley, The ice thickness distribution across the Atlantic sector of the Antarctic Ocean in midwinter, *J. Geophys. Res.*, *92*(C13), 14,535–14,552, 1987.

Wadhams, P., J. C. Comiso, E. Prussen, S. Wells, M. Brandon, E. Aldworth, T. Viehoff, R. Allegrino, and D. R. Crane, The development of the Odden ice tongue in the Greenland Sea during winter 1993 from remote sensing and field observations, *J. Geophys. Res.*, *101*(C8), 18,213–18,235, 1996.

Weeks, W. F., Growth conditions and structure and properties of sea ice, in *Physics of Ice Covered Seas*, edited by M. Lepparanta, pp. 25–105, Univ. of Helsinki, Helsinki, 1998.

Weller, G., Radiation flux investigation, *AIDJEX Bull*, *14*, 28–30, 1972.

M. J. Doble and P. Wadhams, Scottish Association for Marine Science, Dunstaffnage Marine Laboratory, Oban, Argyll PA34 1QA, UK. (majd@dml.ac.uk; Peter.Wadhams@dml.ac.uk)

M. D. Coon, North West Research Associates, Inc., P.O. Box 3027, Bellevue, WA 98009-3027, USA. (max@nwra.com)